Medical Engineering and Physics 37 (2015) 239–244

Contents lists available at ScienceDirect

Medical Engineering and Physics

journal homepage: www.elsevier.com/locate/medengphy

Technical note

Validation of 3D surface reconstruction of vertebrae and spinal column using 3D ultrasound data – A pilot study

Duc V. Nguyen[a], Quang N. Vo[c], Lawrence H. Le[b,c], Edmond H.M. Lou[a,c,*]

[a] Department of Surgery, University of Alberta, Edmonton, Canada
[b] Department of Radiology and Diagnostic Imaging, University of Alberta, Edmonton, Canada
[c] Department of Biomedical Engineering, University of Alberta, Edmonton, Canada

ARTICLE INFO

Article history:
Received 7 November 2013
Revised 12 October 2014
Accepted 29 November 2014

Keywords:
Surface reconstruction
Ultrasound images
Contours stitching
Spine
Vertebra

ABSTRACT

Adolescent idiopathic scoliosis (AIS) is a three-dimensional deformity of spine associated with vertebra rotation. The Cobb angle and axial vertebral rotation are important parameters to assess the severity of scoliosis. However, the vertebral rotation is seldom measured from radiographs due to time consuming. Different techniques have been developed to extract 3D spinal information. Among many techniques, ultrasound imaging is a promising method. This pilot study reported an image processing method to reconstruct the posterior surface of vertebrae from 3D ultrasound data. Three cadaver vertebrae, a Sawbones spine phantom, and a spine from a child with AIS were used to validate the development. The *in-vitro* result showed the surface of the reconstructed image was visually similar to the original objects. The dimension measurement error was <5 mm and the Pearson correlation was >0.99. The results also showed a high accuracy in vertebral rotation with errors of $0.8 \pm 0.3°$, $2.8 \pm 0.3°$ and $3.6 \pm 0.5°$ for the rotation values of 0°, 15° and 30°, respectively. Meanwhile, the difference in the Cobb angle between the phantom and the image was 4° and the vertebral rotation at the apex was 2°. The Cobb angle measured from the *in-vivo* ultrasound image was 4° different from the radiograph.

1. Introduction

Adolescent idiopathic scoliosis (AIS) is a three-dimensional (3D) deformity of spine associated with vertebral rotations [10,23]. Currently, the Cobb method is the gold standard to measure the spinal curvature, called the Cobb angle, on posteroanterior (PA) radiographs. However, this method only shows the spinal curvature on the coronal plane; the axial vertebral rotation and the 3D deformity nature are ignored [5]. Imaging techniques have been developed to extract 3D spinal information. The two most promising techniques are computed tomography (CT) and magnetic resonance imaging (MRI). Both methods can image and display 3D bone structures clearly; however, the CT modality exposes patients to more radiation and requires patients in supine position. Without the gravity effects, the severity of the spinal curvature may alter, which affects the curvature measurement [9]. In addition, using MRI to image spine is costly and time-consuming.

Three-dimensional images of spine can also be obtained from multi-planar standing radiographs. The principle is to identify at least 6 landmarks per vertebra on both PA and lateral radiographs. The direct linear transform [1] technique with these 6 stereo corresponding points (SCPs) is then applied to extract the 3D location information, but this method depends highly on the image quality [19,20]. In addition, some landmarks can only be seen on either the coronal plane or sagittal plane which increases the reconstruction difficulties. Although the non-stereo-corresponding points (NSCP) technique [16] which enables to manually identify landmarks that are only visible in one of the views may solve some of the issue, the operator time increases. Furthermore, researchers had proposed methods for automatically identifying landmarks [2,8,12,17,18,21], but these approaches require a large database as *a priori* knowledge. Recently, an EOS (EOS Imaging, France) system, a medical imaging device, has been reported that it can acquire and display the posteroanterior and lateral X-ray images simultaneously. Researchers reported that this system provided better images and less radiation dosage when compared to the standard radiography [6,14]. However, the EOS method still relies on a database to reconstruct a 3D spine and requires operator to digitize several anatomical landmarks on both PA and lateral radiographs, these are the drawbacks of this method. Furthermore, radiation exposure to patients still exists. In general, during the treatment or monitor periods, AIS patients may take radiographs every 4–12 months [7]; the cumulative amount of ionizing radiation may increase the risk of cancer [7,14,15,24]. Therefore, a non-ionization imaging method is still desirable for scoliosis applications.

* Corresponding author at: Glenrose Rehabilitation Research Center, 10105 112 Ave, Edmonton, AB T5G 0H1, Canada. Tel.: +1 780 735 8212; fax: +1 780 735 7972.
E-mail address: elou@ualberta.ca (E.H. Lou).

http://dx.doi.org/10.1016/j.medengphy.2014.11.007
1350-4533/

Ultrasonography is a non-ionization imaging modality technique that has been used to image scoliotic spine. It is a low cost, portable and real-time medical imaging method. In Chen et al. and Suzuki et al. studies [3,25], spinous processes and laminae were reported as accurate landmarks to assess spinal deformities. The axial rotation of vertebrae was determined by the rotation of the laminae which was parallel to the inclination of the transducer [25]. Meanwhile, Chen et al. [3] proposed the center of lamina method (COL) to estimate the curvature and vertebral rotation of scoliosis in coronal and sagittal planes, respectively. Chen et al. method introduced a reliable measurement which was comparable to the traditional Cobb method. Purnama et al. [22] also introduced a framework to use a freehand 3D ultrasound system to image scoliosis. However, their approach requires a long processing time to display a reconstructed 3D spine. Cheung et al. [4] also used spinous processes and laminae to form a triangle and to display a simple 3D spine structure. A phantom study was performed but the accuracy has not been reported. Another study by Li et al. [13] pointed out that spinous processes could be identified from the ultrasound images and the spinous process angle was highly correlated with the Cobb angle. However, it is known that the high correlation is valid when the rotation of the vertebra is small [11].

From the literature, there is no study applying the surface rendering technique to display 3D reconstruction spine from ultrasound data. This pilot study reported a novel method that could reconstruct the surface of the posterior arch of the vertebrae and spinal column from both *in-vitro* and *in-vivo* 3D ultrasound data. Distance and angle measurements were used to validate the accuracy of reconstructed 3D image. Accurately displaying the 3D spine in a timely manner may provide a better visualization tool for orthopedic surgeons to follow up scoliosis within clinic.

2. Methods

2.1. The equipment

The Ultrasonix SonixTablet (Ultrasonix Ltd., Canada) with a linear probe (L14-5/38 GPS), a built-in magnetic global positioning system (GPS) (SonixGPS) and a 3D Guidance device (driveBAY, Ascension Ltd., USA) (Fig. 1a) were used for data acquisition. The probe frequency can be programmed between 5 and 14 MHz and the depth range can be set between 2 and 9 cm. The active scanning area was 38 mm × 9 mm. The spatial sensor (GPS receiver) embedded inside the linear probe can provide 3D orientation information of each acquired B-scan ultrasound image.

2.2. Experimental setup of cadaveric vertebrae

Three cadaveric vertebrae T7, L1, and L3 were used to validate the developed program. Each vertebra was mounted on a plastic bar with a pointer attached to its center. The plastic bar was then secured on top of a plastic platform (Fig. 1b) which consisted of a protractor to indicate the vertebral rotation. The pivot point was located at the center of mass of the vertebral body. During experiment, the tested vertebrae were submerged into an acrylic water tank with a wall thickness of 4.5 mm. Each vertebra was covered by water (Fig. 1b). The 0° rotation, which was visually aligned, was obtained when the pivot was perpendicular to the surface of the water tank. An ultrasound probe was moved against the wall of the water tank from the top to the bottom of the vertebra, which faced toward the posterior arch of the vertebra. The GPS transmitter was positioned close to the transducer so that the strength of the GPS signal was strong. Two sets of ultrasound data which consisted of ultrasound reflection intensity and position information were exported and processed by the developed image processing program.

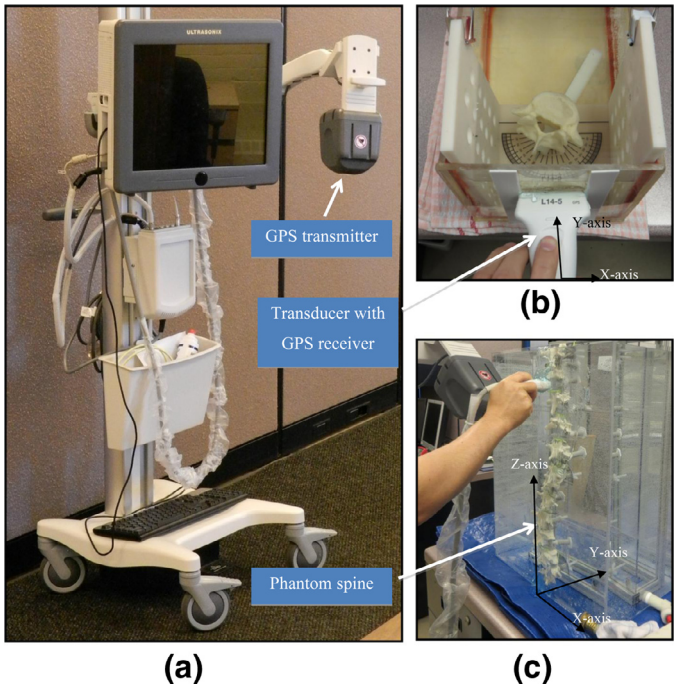

Fig. 1. (a) Ultrasonix SonixTABLET ultrasound scanner with GPS; (b) cadaveric vertebra scanning setup; (c) phantom spine scanning setup.

2.3. Experimental setup for the Sawbones spine phantom

A custom adjustable Sawbones spine phantom consisting of vertebrae from T6 to L5 was also used in this study. Each vertebra of the spine phantom was attached with a transparent protractor to allow axial rotation measurements (Fig. 1c). Three extra protractors were attached to levels T6, T12 and L4 to measure the tilt angles of these 3 vertebrae on the coronal plane. To mimic a scoliotic spine, a smooth axial rotation was set from T7 to T11 and the apex was set at T9 with a value of −20°. The negative value indicated the vertebra was axially rotated to the left. Furthermore, a coronal curve was generated between T7 and T12. The T7 and T12 were the two most tilted vertebrae on the coronal plane with +20° and −30°, respectively. The negative value meant the vertebra was rotated downward and vice versa. The vertebrae between these two vertebrae were adjusted to create a smooth coronal curve. The Cobb angle was the sum of the two most tilted angles, which was 50°. The phantom spine was then submerged into a larger acrylic water tank of dimensions 300 × 400 × 550 mm (Fig. 1c). By using the interface program from the manufacturer, the size of the data acquisition file was limited to 430 Mbytes, which could not store the entire spine image in a single file. To overcome this limitation, four equal section scans with a small overlap between each adjacent section were performed.

2.4. A pilot clinical trial

A girl who has AIS (14.2 years) participated in this study. Local ethics approval was obtained and a written consent was signed. According to her PA radiograph, she had triple curves with apexes at T2, T9 and L3 vertebra levels while the Cobb angles were 26°, 25° and 14°, respectively.

2.5. In-house program

To perform the image processing, a custom program using Microsoft C# and Irrlicht 3D Computer Graphic Engine library was developed to process, reconstruct and display the image. Prior to the

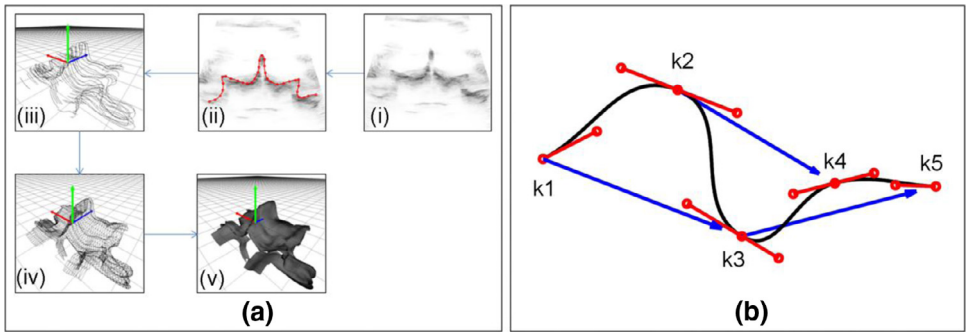

Fig. 2. (a) Surface reconstruction process: (i) B-mode scan, (ii) contour digitization, (iii) contour spatial transformation, (iv) contour triangulation and (v) surface rendering. (b) The Bezier path of five knots k1 to k5.

reconstruction and the display of the surface of each vertebra, this pilot work required the user to digitize the contour of the vertebra on each B-mode ultrasound image frame. This was the most time consuming process, but the goal of this pilot study was to validate 3D surface image was able to be reconstructed. After the digitization, the contour spatial transformation was applied. Surface triangulation and surface rendering were the last 2 steps before displaying the 3D images.

2.5.1. Step 1: Contour digitization

Fig. 2(a)(i) shows a single frame of B-mode ultrasound vertebra image. The contour of the vertebra was digitized manually starting from the left toward the spinous process then to the right (Fig. 2(a)(ii)). Approximately 20 points were digitized, which took 15 s, along the contour of each B-mode image. Since a strong reflection was occurred at the interface between the phantom and water, it was easy to perform this contour segmentation. To smooth the contour and reduce the labor time, the Bézier-spline function (described in Appendix A-I) was applied to generate more points between any two adjacent digitized points. An example of a set of 5 pre-digitized (K_1 to K_5) points is shown in Fig. 2(b).

2.5.2. Step 2: Contour spatial transformation

For each of the cadaveric vertebra, approximately 180 frames of the B-mode images were acquired. Each B-mode image contained a vertebral contour which was a two-dimensional (2D) curve in a 3D space. The location and orientation of each 2D curve were recorded relative to the center of the GPS transmitter (global coordinate [0,0,0]). To stack the 180 vertebral contours together, the following process was applied to place the 2D curves into 3D space (Fig. 2(a)(iii)).

Let R_{tl}, R_{tr}, R_{bl} be the 3D coordinates of the top-left, top-right, bottom-left corners of the B-scan frame, respectively. The unit vectors along the x-axis and y-axis can be calculated as:

$$\overrightarrow{ux} = \frac{\overrightarrow{R_{tr}} - \overrightarrow{R_{tl}}}{\left\|\overrightarrow{R_{tr}} - \overrightarrow{R_{tl}}\right\|} \quad \overrightarrow{uy} = \frac{\overrightarrow{R_{bl}} - \overrightarrow{R_{tl}}}{\left\|\overrightarrow{R_{bl}} - \overrightarrow{R_{tl}}\right\|} \tag{1}$$

The 3D coordinate (x', y', z') of point (x, y) on the B-scan plane can be obtained by using Eq. (2):

$$p = \overrightarrow{ux} * x + \overrightarrow{uy} * y + \overrightarrow{R_{tl}} \tag{2}$$

2.5.3. Step 3: Contour triangulation

After the 3D space contour was constructed, triangles were created among three vertices of two neighboring contours to form 3D meshes. Let $P = \{p_1, \ldots, p_m\}$ and $Q = \{q_1, \ldots, q_n\}$ were registered point sets of two consecutive contours P and Q, respectively. The program was then created the set of triangles $T = \{t_1, \ldots, t_k\}$ that constituted the mesh between two contours P and Q. The quality of the reconstructed surface depended on how the T set was built. There were four constraints that each triangle $t_i \in T$ had to satisfy: (i) two of the three vertices needed to belong to one contour; the other had to belong to the other contour. This condition was to ensure that the mesh was created between two adjacent contours, not on a single contour itself; (ii) the two vertices that belonged to the same contour had to be situated next to each other; (iii) the triangles did not overlap; (iv) the area of triangles should be as small as possible. This condition was to ensure that the mesh only spanned between two closest contour segments.

The first three conditions can be expressed in Eq. (3) as follows:

$$t_i = \begin{cases} \{p_u, q_v, p_{u+1}\} \wedge \{p_u, p_{u+1}\} \notin t_{j \neq i} \\ \{p_u, q_v, q_{v+1}\} \wedge \{q_v, q_{v+1}\} \notin t_{j \neq i} \end{cases} \tag{3}$$

The algorithm for calculating set T which satisfies (3) is described in Algorithm 1 (Appendix A-II).

Fig. 2(a)(iv) shows the image of the vertebral triangulation.

2.5.4. Step 4: Surface rendering

According to the resolution of the ultrasound probe, the distance between two consecutive frames of a B-mode image was approximately 0.7 mm. The mesh surface was then applied to rendering the triangular surface (Fig. 2(a)(v)).

2.6. Calibration

For the phantom study, the surface of the scanning acrylic walls was used as the reference plane. Referring to Fig. 1(b) and (c), the X-axis is parallel to the left and right direction, the Y-axis is perpendicular to the scanning wall and the Z-axis is parallel to the up and down direction. For the pilot clinical case, we used the last frame of the ultrasound image that was able to identify the center of laminae to be the reference plane. The X-, Y- and Z-axes were similar to the phantom study shown in Fig. 1(c). The last frame was at the L5 level. A line connected the two centers of laminae was the X-axis. A line joining the tip of the spinous process on the last few frames and perpendicular to the X-axis was the Z-axis. The Y-axis was perpendicular to both X- and Z-axes. The assumption of this was the last vertebra should have minimal axial vertebral rotation.

2.7. Validation

To evaluate the accuracy of the surface reconstruction, two raters measured the dimensions and angles from the cadaveric vertebrae (T7, L1 and L3) and the corresponding surface images twice in one week apart to minimize memory bias. To measure the real dimensions of the cadaveric vertebra, a digital caliper (Digimatic, Mitutoyo Corporation, Japan) was used. To measure the reconstructed 3D images, the raters used the computer mouse pointer to locate two endpoints of each corresponding distance. Three repeated measurements were performed at each time. The distance measurements were (a) between two transverse processes, (b) between two laminae,

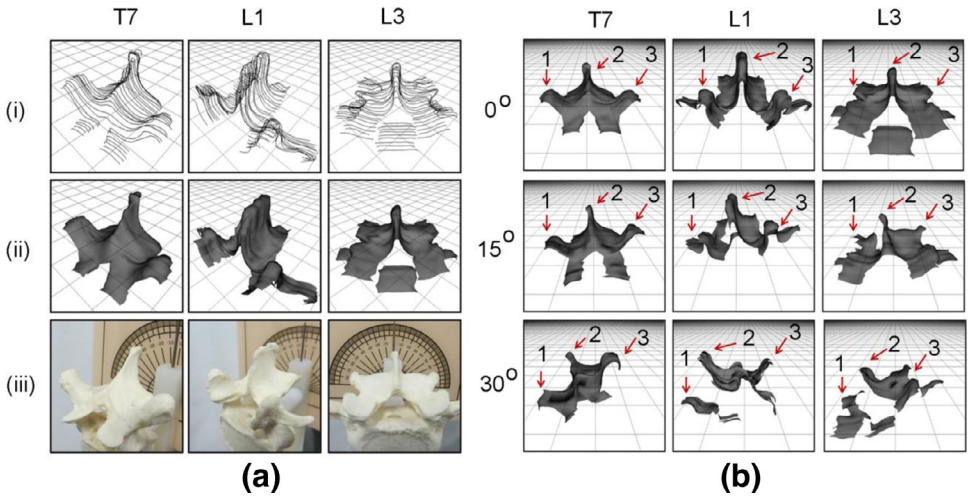

Fig. 3. (a) Surface reconstruction of cadaveric vertebrae at 0° rotation at different view angles. Row (i) The stack of spatial transformed contours, (ii) the reconstructed surfaces of single vertebra, (iii) the cadaveric vertebrae. (b) Surface reconstruction of the cadaveric vertebrae with axial rotation at 0°, 15°, and 30°. Labels 1 and 3 are the transverse processes and label 2 is the spinous process.

(c) between the right superior articular process and the right inferior articular process, and (d) between the left superior articular process and the left inferior articular process. Therefore, 12 measured values (3 measures × 2 times × 2 raters) were obtained on each parameter. The mean absolute difference between the image and the cadaveric measurements were calculated and the overall Pearson correlation on each of the vertebra was determined. The intra- and inter-correlation coefficients of the dimensions measurements [ICC(2,1)] using a two-way random model and absolute agreement with interval of 95% were calculated. Furthermore, the three vertebral rotation angles in the cadaveric vertebrae experiments were set to 0°, 15°, and 30° for each of the vertebra (T7, L1 and L3) based on the attached protractors. Since the wall of the water tank was perpendicular to the pivot at 0° of the vertebral rotation, the reconstructed 3D vertebra relative to the tank surface was used to represent the rotation of the vertebra. To measure the rotation angles from the reconstructed surface vertebrae, a virtual camera was set at a location so that it would provide a correct image scale. The horizontal reference was parallel to the frame of each B-mode image. The projected image was then captured as an input image to the ImageJ software (National Institutes of Health, USA) to measure the rotation angle.

For the reconstructed spine phantom, the method to measure the axial rotation angle of T9 was the same as the cadaveric vertebra method. To measure the Cobb angle, since the endplates of each vertebra could not be identified, the center of lamina method [3] was used. Each rater had to draw lines on the two most tilted vertebrae along the curve and each line needed to pass through the centers of laminae of the selected vertebrae. This method was also applied to the *in-vivo* data to measure the Cobb angle.

3. Results

Fig. 3a shows the results of the surface reconstruction of T7, L1 and L3 at 0° rotation in columns 1, 2, and 3, respectively. On row (i), it shows the stacks of spatial transformed contours; on row (ii) it is the reconstructed vertebrae (surface rendering) and on row (iii) it shows the cadaveric vertebrae. Fig. 3b shows the reconstructions of T7, L1 and L3 at 0°, 15° and 30° rotation. Due to the rotation of the vertebra, some of the surface details were missing because some of the ultrasound signals were blocked by the spinous process, especially in L1 and L3, their spinous processes are bigger than that of T7. Fig. 4 shows the reconstruction of the spine and compares with the spine phantom. Fig. 5 shows the reconstructed spine from the AIS subject. Fig. 5d shows a reconstructed surface image overlaid on the radiograph.

Table 1a shows the comparison of the four aforementioned distance measurements on both cadaveric vertebrae and reconstructed images. All the values in the table are mean ± standard deviation of 12 measurements. Overall, the mean absolute difference of the distance measurements between the cadaveric and reconstructed images was less than 5 mm. The Pearson correlation was greater than 0.99. The intra- and inter-correlation coefficients of the dimensions measurements were 0.95 and 0.90, respectively, which meant high reliability to measure. The comparisons of axial rotation angles between the phantom vertebrae and the image are illustrated in Table 1b. The average difference ± the standard deviation of the vertebral rotation at 0°, 15° and 30° are 0.8 ± 0.3°, 2.8 ± 0.3° and 3.6 ± 0.5°, respectively. The larger the rotation angle, the higher the measurement error. Furthermore, the rotation angles between the phantom spine and the reconstructed measurements are summarized in Table 2. The difference of the vertebral rotation at the apex was approximately 2 ± 1.1°, which was similar to the single vertebra measurement. The phantom Cobb angle was 46 ± 2.3° versus the preset 50°. The Cobb angles from the reconstructed ultrasound image were 23°, 24° and 10° and they were only measured by one rater who was blinded to the clinical information at one time.

4. Discussions

In this study, we successfully reconstructed the 3D surface of the posterior arch of vertebrae, spine phantom and a spine from an AIS patient. Although the quality of the 3D ultrasound spine image is not as good as the CT and MRI, the required information is able to be measured. Furthermore, the surface of the reconstructed image was visually similar to the original object. The results summarized in Table 2 demonstrate a good reconstruction of the whole spine with a difference of 4° in Cobb angles and 2° in vertebral rotation. To truly validate the measurement accuracy, more patients' data are required.

However, there are some limitations in this study due to the characteristic of the ultrasound. Firstly, this method cannot image and display vertebral body due to the acquisition configuration and the lack of ultrasound energy penetrating through bone. As a result, this limits using the Cobb method to measure the Cobb angle. Secondly, when the axial vertebral rotation is large, some of the areas behind the spinal process (white space in Fig. 3b) have no ultrasound signal. The reason is the side of the spinous process facing toward the

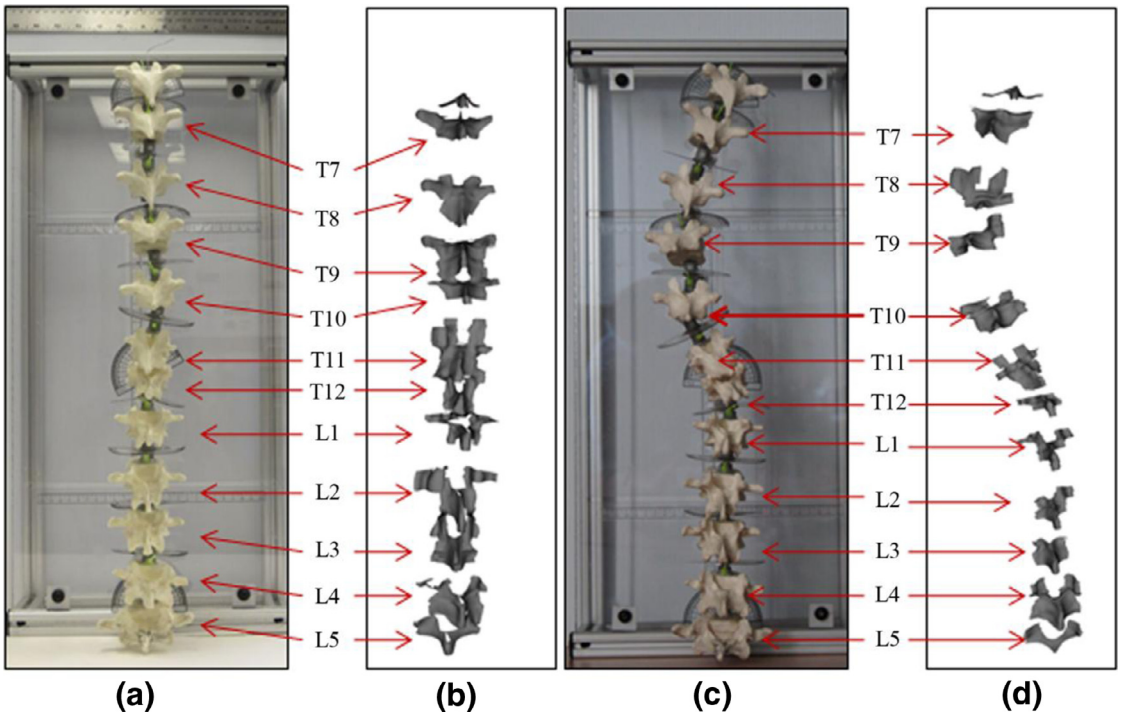

Fig. 4. (a) The phantom spine with 0° Cobb angle configuration, (b) the surface reconstructed spine with 0° Cobb angle, (c) the phantom spine with 50° Cobb angle configuration and (d) the surface reconstructed spine with 50° Cobb angle.

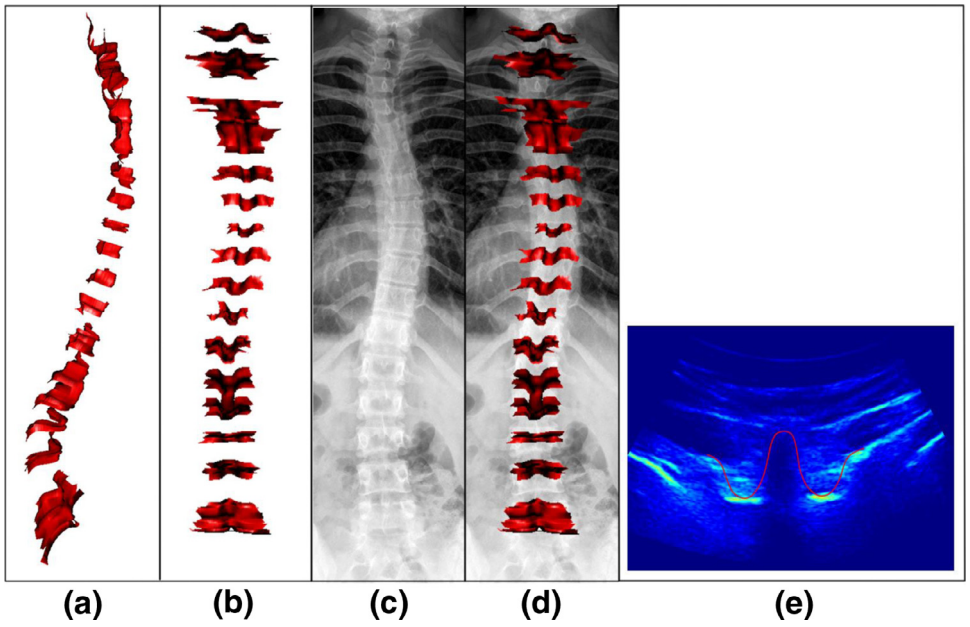

Fig. 5. Surface reconstruction of spine on vivo data: (a) sagittal view of the reconstructed spine, (b) coronal view of reconstructed spine, (c) X-ray image of the tested subject, (d) overlay the reconstructed image on radiograph, and (e) a B-frame image with w-shape of bone surface drawn by a rater.

transducer blocks the emitted ultrasound signals. Thirdly, the developed method needs an operator to manually identify the contours of the vertebrae surface on each B-mode image and to perform digitization. For the 3D spine phantom, approximately 850 B-mode images were captured and the distance between each frame was 0.7 mm. To fully digitize the 850 B-mode images, 5 h will be required. In this study, we only used 170 B-mode images, which still required an hour to digitize along the contours. Using 1/5 of the captured frames, the resolution became 3.5 mm. However, the resolution of the reconstructed spine was not that important because the main purpose was to demonstrate that 3D spine surface could be reconstructed. For the *in-vivo* spine, 1121 B-mode images were captured and 224 images were digitized. Automatic trace and pattern recognition algorithms will be developed in the future to speed up the digitization process. Next, the number of test subjects is small. The future step is to collect more patient data to validate the development. Finally, using vertebra L5 as the reference coordinate system may not be feasible and accurate in real situation. Further research is needed to investigate a better coordination system for this ultrasound imaging method.

Table 1a
Comparisons of distance measurements between individual cadaveric vertebrae and images.

Vertebra		Lamina–Lamina (mm)	TP–TP (mm)	LSAP–LSIP (mm)	RSAP–RSIP (mm)	Pearson correlation
T7	Image	21.5 ± 1.0	45.9 ± 1.4	30.9 ± 0.3	31.2 ± 0.5	0.991
	Cadaver	18.7 ± 1.0	46.1 ± 0.9	29.1 ± 0.3	29.1 ± 0.6	
	MAD	2.8 ± 1.8	1.4 ± 1.1	1.7 ± 0.5	2.0 ± 0.7	
L1	Image	16.8 ± 0.7	60.2 ± 0.5	38.1 ± 0.5	38.9 ± 0.4	0.992
	Cadaver	15.2 ± 0.7	60.4 ± 0.6	42.1 ± 0.4	41.2 ± 0.5	
	MAD	1.6 ± 1.0	0.5 ± 0.3	4.1 ± 0.6	2.3 ± 0.7	
L3	Image	19.4 ± 1.0	68.6 ± 0.7	40.7 ± 0.3	41.3 ± 0.2	0.992
	Cadaver	18.7 ± 0.6	68.4 ± 0.9	36.3 ± 0.2	36.6 ± 0.5	
	MAD	1.0 ± 0.7	1.1 ± 0.6	4.4 ± 0.3	4.7 ± 0.7	

TP: transverse processes; L/R SAP: left/right superior articular process; L/R IAP: left/right inferior articular process; MAD: mean absolute difference.

Table 1b
Comparisons of angle measurements between individual cadaveric vertebrae and images.

Vertebra	Axial rotation angle (°)		
	0	15	30
T7	2.3 ± 0.9	16.1 ± 2	34.3 ± 1.3
L1	−0.6 ± 2	18.5 ± 1.4	34.5 ± 4.2
L3	0.8 ± 1.8	18.8 ± 1.2	32.0 ± 0.8
Mean ± SEM	0.8 ± 0.3	2.8 ± 0.3	3.6 ± 0.5

SEM: standard error mean.

Table 2
Comparisons of measurements between the spine phantom and images.

Vertebra	T7	T9	T11
Preset axial rotation angle (°)	5	−20	0
Measured mean ± SD of axial rotation (°)	−1 ± 1.1	−22 ± 1.1	2.7 ± 2.1
Preset Cobb angle (°): 50	Measured Cobb angle (°): 46 ± 2.3		

Funding

None.

Ethical approval

Ethical approval was granted from the Health Research Ethics Board at the University of Alberta. The reference number is Pro00005707.

Conflict of interest

None declared.

Supplementary materials

Supplementary material associated with this article can be found, in the online version, at doi:10.1016/j.medengphy.2014.11.007.

References

[1] Aziz A, Karara HM. Direct linear transformation into object space coordinates in close-range photogrammetry. In: Proceedings of the symposium on close-range photogrammetry. Illinois: Urbama; 1971. p. 1–18.
[2] Benameur S, Mignotte M, Labelle H, De Guise JA. A hierarchical statistical modeling approach for the unsupervised 3-D biplanar reconstruction of the scoliotic spine. IEEE Trans Biomed Eng 2005;52:2041–57.
[3] Chen W, Le LH, Lou EHM. Ultrasound imaging of spinal vertebra to study scoliosis. Open J Acoust 2012;2:95–103.
[4] Cheung CWJ, Zheng Y. Development of 3-D ultrasound system for assessment of adolescent idiopathic scoliosis (AIS). In: Lim CT, Goh JCH, editors. Proceedings of the 6th World Congress of Biomechanics. Singapore: International Federation for Medical and Biological Engineering; 2010. p. 584–7.
[5] Deacon P, Flood BM, Dickson RA. Idiopathic scoliosis in three dimensions: a radiographic and morphometric analysis. J Bone Joint Surg Br 1984;66:509–12.
[6] Deschenes S, Charron G, Beaudoin G, Labelle H, Dubois J, Miron MC, et al. Diagnostic imaging of spinal deformities: reducing patients radiation dose with a new slot-scanning X-ray imager. Spine 2010;35:989–94.
[7] Doody MM, Lonstein JE, Stovall M, Hacker DG, Luckyanov N, Land CE. Breast cancer mortality after diagnostic radiography: findings from the U.S. scoliosis cohort study. Spine 2000;25:2052–63.
[8] Dumas R, Blanchard B, Carlier R, de Loubresse CG, Le Huec JC, Marty C, et al. A semi-automated method using interpolation and optimisation for the 3D reconstruction of the spine from bi-planar radiography: a precision and accuracy study. Med Biol Eng Comput 2008;46:85–92.
[9] Forsberg D, Lundstrom C, Andersson M, Vavruch L, Tropp H, Knutsson H. Fully automatic measurements of axial vertebral rotation for assessment of spinal deformity in idiopathic scoliosis. Phys Med Biol 2013;58:1775–87.
[10] Graf H, Hecquet J, Dubousset J. 3-dimensional approach to spinal deformities. Application to the study of the prognosis of pediatric scoliosis. Rev Chir Orthop Reparatrice Appar Mot 1983;69:407–16.
[11] Herzenberg JE, Waanders NA, Closkey RF, Schultz AB, Hensinger RN. Cobb angle versus spinous process angle in adolescent idiopathic scoliosis. The relationship of the anterior and posterior deformities. Spine 1990;15:874–9.
[12] Kadoury S, Cheriet F, Labelle H. A statistical image-based approach for the 3D reconstruction of the scoliotic spine from biplanar radiographs. In: Proceedings of the 5th IEEE international symposium on biomedical imaging Paris; 2008. p. 660–3.
[13] Li M, Cheng J, Ying M, Ng B, Zheng YP, Lam TP, et al. Could clinical ultrasound improve the fitting of spinal orthosis for the patients with AIS?. Eur Spine J 2012;21:1926–35.
[14] McKenna C, Wade R, Faria R, Yang H, Stirk L, Gummerson N, et al. EOS 2D/3D X-ray imaging system: a systematic review and economic evaluation. Health Technol Assess 2012;16:11–17.
[15] Miller NH. Cause and natural history of adolescent idiopathic scoliosis. Orthop Clin North Am 1999;30:343–52.
[16] Mitton D, Landry C, Veron S, Skalli W, Lavaste F, De Guise JA. 3D reconstruction method from biplanar radiography using nonstereo corresponding points and elastic deformable meshes. Med Biol Eng Comput 2000;38:133–9.
[17] Mitulescu A, Semaan I, De Guise JA, Leborgne P, Adamsbaum C, Skalli W. Validation of the non-stereo corresponding points stereoradiographic 3D reconstruction technique. Med Biol Eng Comput 2001;39:152–8.
[18] Moura DC, Boisvert J, Barbosa JG, Labelle H, Tavares JM. Fast 3D reconstruction of the spine from biplanar radiographs using a deformable articulated model. Med Eng Phys 2011;33:924–33.
[19] Nyström L, Söderkvist I, Wedin P-Å. A note on some identification problems arising in roentgen stereo photogrammetric analysis. J Biomech 1994;27:1291–4.
[20] Pearcy MJ. Stereo radiography of lumbar spine motion. Acta Orthop Scand Suppl 1985;212:1–45.
[21] Pomero V, Mitton D, Laporte S, de Guise JA, Skalli W. Fast accurate stereoradiographic 3D-reconstruction of the spine using a combined geometric and statistic model. Clin Biomech 2004;19:240–7.
[22] Purnama KE, Wilkinson MH, Veldhuizen AG, van Ooijen PM, Lubbers J, Burgerhof JG, et al. A framework for human spine imaging using a freehand 3D ultrasound system. Technol Health Care 2010;18:1–17.
[23] Roaf R. Rotation movements of the spine with special reference to scoliosis. J Bone Joint Surg Br 1958;40:312–32.
[24] Ronckers CM, Land CE, Miller JS, Stovall M, Lonstein JE, Doody MM. Cancer mortality among women frequently exposed to radiographic examinations for spinal disorders. Radiat Res 2010;174:83–90.
[25] Suzuki S, Yamamuro T, Shikata J, Shimizu K, Iida H. Ultrasound measurement of vertebral rotation in idiopathic scoliosis. J Bone Joint Surg Br 1989;71:252–5.